

Tensorized Incomplete Multi-View Clustering with Intrinsic Graph Completion

Shuping Zhao^{1†}, Jie Wen^{2†}, Lunke Fei³, Bob Zhang^{1*}

¹PAMI Research Group, Department of Computer and Information Science, University of Macau, Taipa, Macau

²Shenzhen Key Laboratory of Visual Object Detection and Recognition, Harbin Institute of Technology, Shenzhen, Shenzhen, 518055, China

³School of Computer Science, Guangdong University of Technology, Guangzhou, 510006, China.
yb77458@um.edu.mo, jiewen_pr@126.com, flksxm@126.com, bobzhang@um.edu.mo

Abstract

Most of the existing incomplete multi-view clustering (IMVC) methods focus on attaining a consensus representation from different views but ignore the important information hidden in the missing views and the latent intrinsic structures in each view. To tackle these issues, in this paper, a unified and novel framework, named tensorized incomplete multi-view clustering with intrinsic graph completion (TIMVC_IGC) is proposed. Firstly, owing to the effectiveness of the low-rank representation in revealing the inherent structure of the data, we exploit it to infer the missing instances and construct the complete graph for each view. Afterwards, inspired by the structural consistency, a between-view consistency constraint is imposed to guarantee the similarity of the graphs from different views. More importantly, the TIMVC_IGC simultaneously learns the low-rank structures of the different views and explores the correlations of the different graphs in a latent manifold sub-space using a low-rank tensor constraint, such that the intrinsic graphs of the different views can be obtained. Finally, a consensus representation for each sample is gained with a co-regularization term for final clustering. Experimental results on several real-world databases illustrates that the proposed method can outperform the other state-of-the-art related methods for incomplete multi-view clustering.

Introduction

In recent years, multi-view clustering (MVC) has become attractive, where it has been applied to a variety of applications, i.e., image retrieval, webpage retrieval, and speech recognition (Huang, Zhang, and Pižurica 2021; Mitra et al. 2018; Xu et al. 2022; Cui et al. 2020). Since features collected from multiple views contain more complementary information, MVC has the potential to gain a better performance than single-view clustering (Tao et al. 2018; Chao, Sun, and Bi 2021; Wang et al. 2021a). Up to now, a variety of MVC methods have achieved significant performances, such as structured low-rank matrix factorization based MVC (Wang et al. 2018), agglomerative neural networks for MVC (Liu et al. 2021), parameter-free consensus embedding learning based IMVC (Wu et al. 2021), joint

partition and graph learning based IMVC (Li, Wan, and He 2021), and deep multiview clustering (Zhang et al. 2021). Commonly, these MVC methods require that all views are complete. Nevertheless, due to the fact that many reasons can bring about the deficiency of the views, such as data corruption, breakdown of the sensors, the privacy policies, etc., the incomplete multi-view data causes a view-missing challenge in MVC tasks, called incomplete multi-view clustering (IMVC). The conventional MVC methods will be invalid for the IMVC tasks, since some instances from some views are missing (Wen et al. 2020a; Xu et al. 2021; Wen et al. 2022).

Some problems may arise in the IMVC applications, on account of the missing view: 1) The multi-view data cannot provide complete views for the exploration of the complementary information; 2) The broken data causes a serious imbalance problem, owing to the fact that the views may have several numbers of features. Some researchers have made many efforts to tackle these demanding IMVC issues. For instance, Wen et al. (Wen et al. 2020a) proposed an adaptive graph completion based method, Zhao et al. (Zhao et al. 2021) proposed an intrinsic and complete structure inferring strategy, and Xia et al. (Xia et al. 2022) proposed a tensor completion based method. Generally, the existing IMVC methods can be divided into two categories according to their exploited techniques, i.e., matrix factorization-based IMVC (MF_IMVC) and graph learning-based IMVC (GL_IMVC). MF_IMVC seeks to learn a low-dimensional consensus representation from the original multi-view data adopting the matrix factorization approach. In this way, partial MVC will learn a common latent sub-space for all views, such that instances from different views could share a same low-dimensional representation (Li, Jiang, and Zhou 2014). However, partial PMVC could only handle the incomplete multi-view data with two views. Different from Partial MVC, Shao et al. (Shao, He, and Yu 2015a) filled the absent instances with the average value of the collected data for their corresponding view. However, this simple data completion strategy easily leads to the over-fitting problem, since the intrinsic structure is ignored.

Many GL_IMVC based methods have also been proposed for more flexible application scenarios. Specifically, GL_IMVC desires to produce a consensus representation from multiple graphs constructed from different views,

*indicates the corresponding author; † indicates the co-first authors.

Copyright © 2023, Association for the Advancement of Artificial Intelligence (www.aaai.org). All rights reserved.

which can characterize the local structures of the data (Wen, Xu, and Liu 2018; Zhao et al. 2021). For example, Wang et al. (Wang et al. 2019) proposed a perturbation-oriented IMVC method, that learned a consensus representation from pre-defined similar graphs from different views. Besides this, in (Wen et al. 2020b), a graph-regularized matrix factorization strategy was developed for local geometric structure preserving, then a common representation was learned for clustering. However, these methods are troubled with a restriction that the incomplete graphs constructed from the defective views cannot provide unabridged relationships of samples. To solve this problem, some graph completion-based IMVC methods have been proposed. For instance, Wen et al. (Wen et al. 2020a) proposed an adaptive graph completion based method, which learned the complete graphs by adopting two constraints of within-view preservation and between-view inferring. Nevertheless, the pre-defined graphs of multiple views could not reflect the intrinsic structures of the data.

From the analysis of the aforementioned IMVC methods, two defects still limit the performance in IMVC tasks (Lu et al. 2019; Wang et al. 2021b; Hu, Lou, and Ye 2021). On the one hand, existing methods neglect the important information hidden in the missing views. On the other hand, the consistency of the structures from different views is not considered in the iterative learning procedure. To tackle these issues, in this paper, a novel missing view inferring based IMVC model, named TIMVC_IGC is proposed. Specifically, owing to the effectiveness of low-rank representation in revealing the inherent structure of the data, we first exploit it to infer the missing instances and construct the complete graph for each view. Afterwards, inspired by the structural consistency, a between-view consistency constraint is imposed to improve the similarity of the graphs from different views. In this way, TIMVC_IGC simultaneously learns the low-rank structures and explores the correlations of different graphs in a latent manifold sub-space using a low-rank tensor constraint, such that the intrinsic graphs of different views can be obtained. Finally, a low-dimensionality consensus representation shared by all views is learned for each sample using a co-regularization term. The main contributions of the proposed method can be briefly summarized as follows:

1) The proposed TIMVC_IGC provides a novel and effective approach for all kinds of incomplete multi-view clustering cases, which sufficiently explores the recovered full information and the correlative structure learning of different views for intrinsic graph construction.

2) A tensor low-rank regularization is introduced to learn the structures of the recovered complete data for different views, where a between-view preserving constraint is also proposed to enhance the similarity of the different graphs. In such a manner, the intrinsic structures can be constructed and preserved in different views.

Preliminaries

Spectral clustering aspires to capture a graph from the data points for clustering, where the graph can characterize the inherent correlations between different data points (Zhu

et al. 2018; Sharma and Seal 2021). For multi-view clustering, a general approach is to learn a consistency representation of the multiple graphs learned from different views. For examples, Gao et al. (Gao et al. 2015) proposed a classical multi-view clustering model for the consensus representation learning as follows:

$$\min_F \sum_{v=1}^V Tr(F^T L_{S^{(v)}} F) \text{ s.t. } F^T F = I \quad (1)$$

where $F \in R^{n \times c}$ denotes the consensus representation of the different views, n indicates the number of subjects, c is the cluster number, and $L_{S^{(v)}}$ denotes the Laplacian matrix of the graph $S^{(v)}$. In particular, $L_{S^{(v)}}$ is attained by $L_{S^{(v)}} = D^{(v)} - (S^{(v)} + S^{(v)})/2$, where $D^{(v)}$ denotes a diagonal matrix that the i th diagonal element is computed as $D_{i,i}^{(v)} = \sum_{j=1}^V (S_{i,j}^{(v)} + S_{j,i}^{(v)})/2$.

To capture the higher-order correlations between the adjacency graphs from different views, especially for original spatial structure, it is desirable that third-order tensors can be operated like matrices using linear algebra tools. The tensor nuclear norm is defined as follows (Wen et al. 2021; Wu et al. 2020; Cheng, Jing, and Ng 2018):

Definition 1 For a tensor $D \in R^{n_1 \times n_2 \times n_3}$, the t-SVD based tensor nuclear norm is defined as:

$$\|D\|_{\otimes} = \sum_{k=1}^{n_3} \|D_f^{(k)}\|_* = \sum_{i=1}^{\min(n_1, n_2)} \sum_{k=1}^{n_3} |S_f^{(k)}(i, i)|$$

where D_f is the fast Fourier transformation (FFT) of tensor D along the third dimension, i.e., $D_f = \text{fft}(D, [], 3)$. $\|D_f^{(k)}\|_*$ presents the nuclear norm of the k th frontal slice of tensor D_f . $S_f^{(k)}(i, i)$ is the i th singular value of $D_f^{(k)}$ calculated by SVD on $D_f^{(k)}$ like

$$D_f^{(k)} = U_f^{(k)}(i, i) S_f^{(k)}(i, i) V_f^{(k)}(i, i)^T.$$

The Proposed Method

Fig. 1 shows some cases of the multi-view data. For the unbroken multi-view data, the paired instances from all views are complete. Case 1 - Case 3 present the varying degrees of the instance missing for different views. Specifically, in Case 3 features from more than two views are arbitrarily missing.

Model of TIMVC_IGC

Graph learning based methods have achieved positive performances in clusterig, which aims to capture the intrinsic structure of the data (Pan and Kang 2021; Zhang et al. 2022; Chen et al. 2021; Zhu et al. 2022). In such a manner, the correlations between each two arbitrary data points can be attained. From the previous analysis, it can be seen that low-rank representation is an effective approach for drawing such a graph. Let $\{\tilde{X}^{(v)} \in R^{d^{(v)} \times n}\}_{v=1}^V$ denote a multi-view data set, where V represents the number of views, $d^{(v)}$ is the feature dimensionality of the v th view, and n is the total number of data points. Then, we can construct the naive low-rank representation for each view of \tilde{X} as follows:

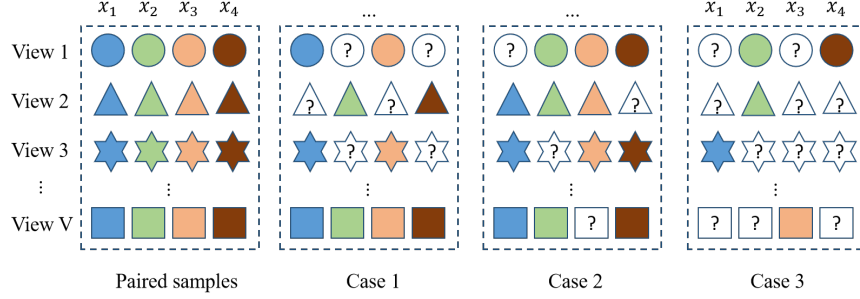


Figure 1: Some cases of multi-view data with different degrees of missing samples for each view.

$$\min_{Z^{(v)}} \sum_{v=1}^V \|Z^{(v)}\|_* + \lambda \|B^{(v)}\|_1 \quad (2)$$

$$s.t. \tilde{X}^{(v)} = \tilde{X}^{(v)} Z^{(v)} + B^{(v)}, \text{diag}(Z^{(v)}) = 0,$$

where $Z^{(v)} \in R^{n \times n}$ is the low-rank representation matrix, $E^{(v)} \in R^{d^{(v)} \times n}$ characterizes the noise in each view, and $\lambda \geq 0$ is a penalty parameter.

Formula (2) requires that all views of \tilde{X} are complete, which will be invalid for a IMVC task, since graphs constructed from the incomplete views still have different sizes (Abhadiomhen et al. 2021; Jia et al. 2021; Hu, Shi, and Ye 2020). Many researchers fill in the absent instances with the average feature vector of the corresponding view (Gao, Peng, and Jian 2016). However, these filled instances will be regarded as the same classes contributing error connected weights to the construction of the graph. In contrast, the completion graph can be learned by exploiting the retained structure information from the other views (Wen et al. 2020a; Li and He 2020). However, the incomplete problem of paired instances for each of the two samples will lead to the failure of this method in the case that the incomplete paired instances cannot be utilized to calculate the connected weights for all views. To handle the incomplete multi-view data, where each view has the potential to be lost, we introduce a missing view inferring strategy integrating the intrinsic graph learning for each view as follows:

$$\min_{Z^{(v)}, E^{(v)}} \sum_{v=1}^V \|Y^{(v)} - Y^{(v)} Z^{(v)}\|_1 + \lambda_1 \|E^{(v)}\|_F^2 + \lambda_2 \|W^{(v)}\|_F^2 + \lambda_3 \|Z\|_* \quad (3)$$

$$s.t. Y^{(v)} = X^{(v)} + E^{(v)} W^{(v)}, Z^{(v)} \geq 0, \text{diag}(Z^{(v)}) = 0, Z^{(v)} I = I$$

where $X^{(v)} \in R^{d^{(v)} \times n}$ and $E^{(v)} \in R^{d^{(v)} \times n^{(v)}}$ represent the collected instances and absent instances as well as the reconstructed missing instances from the v th view, respectively. Besides this, λ_1 , λ_2 , and λ_3 are the nonnegative penalty parameters. $Z^{(v)} I = I$ guarantees that all instances from different views can be connected with at least on instance. In particular, the missing instances in $X^{(v)}$ are filled as zero vectors. In addition, $W^{(v)} \in R^{n^{(v)} \times n}$ signifies a prior mapping matrix that projects the missing instance matrix to the

recovered complete data matrix in its corresponding locations as follows:

$$W_{i,j}^{(v)} = \begin{cases} 1, & \text{if the } i\text{th missing instance is } x_j^{(v)} \\ 0, & \text{otherwise.} \end{cases} \quad (4)$$

where $x_j^{(v)}$ indicates the j th instance of the v th view.

Overall Objective Function Though formula (3) can learn a complete graph by recovering the missing instances for each view, the correlations between different views is still neglected, such that the complementary information retained by each view cannot be fully utilized. Furthermore, we also need to consider the semantic consistency hidden in different views, so as to guarantee that all views can have a similar clustering decision. To address these problems, we propose a tensor based TIMVC_IGC framework for spectral clustering as follows:

$$\min_{Z^{(v)}, E^{(v)}, H, F} \sum_{v=1}^V \|Y^{(v)} - Y^{(v)} Z^{(v)}\|_1 + \sum_{v=1}^V \left(\lambda_1 \|Z^{(v)} - \sum_{i=1, i \neq v}^V Z^{(i)} H_{i,v}\|_F^2 + \lambda_2 \|E^{(v)}\|_F^2 \right) + \sum_{v=1}^V \lambda_3 \text{Tr}(F^T L_{Z^{(v)}} F) + \|Z\|_{\otimes} \quad (5)$$

$$s.t. Y^{(v)} = X^{(v)} + E^{(v)} W^{(v)}, Z^{(v)} \geq 0, \text{diag}(Z^{(v)}) = 0, Z^{(v)} I = I, F^T F = I, 0 \leq h_{i,v} \leq 1, \sum_{i=1, i \neq v}^V H_{i,v} = 1, H_{v,v} = 0.$$

where $H \in R^{V \times V}$ is the self-representation matrix, $F \in R^{n \times c}$ denotes the consistency representation, and c is the dimensionality of each representation vector in F .

Specifically, the tensor low-rank constraint $\|Z\|_{\otimes}$ can crucially capture the higher-order correlations between different views (Zhang et al. 2020). Besides this, the between-view preserving constraint $\|Z^{(v)} - \sum_{i=1, i \neq v}^V Z^{(i)} H_{i,v}\|_F^2$ can enhance the similarity of different graphs by adopting the complementary information from each view. After the intrinsic graphs have been attained for different views, we can learn the semantic consistency representation F shared by all views for final spectral clustering.

Solution to TIMVC_IGC

In this sub-section, we exploit the ALM strategy (Zhang et al. 2017) to alternatively achieve the optimum solution for each variable of (5). To make (5) separable, the auxiliary variables $B^{(v)}$ and \mathcal{P} are introduced to (6) and the augmented Lagrangian function is re-formulated as follows:

$$\min_{\psi} \sum_{v=1}^V \left(\begin{array}{l} \|B^{(v)}\|_1 + \lambda_2 \|E^{(v)}\|_F^2 \\ + \lambda_1 \|Z^{(v)} - \sum_{i=1, i \neq v}^V Z^{(i)} H_{i,v}\|_F^2 \\ + \lambda_3 \text{Tr}(F^T L_{Z^{(v)}} F) + \\ \frac{\mu}{2} \|Y^{(v)} - X^{(v)} - E^{(v)} W^{(v)} + \frac{C_1^{(v)}}{\mu}\|_F^2 \\ + \frac{\mu}{2} \|Y^{(v)} - Y^{(v)} Z^{(v)} - B^{(v)} + \frac{C_2^{(v)}}{\mu}\|_F^2 \\ + \frac{\mu}{2} \|Z^{(v)} - P^{(v)} + \frac{C_3^{(v)}}{\mu}\|_F^2 \end{array} \right) + \|\mathcal{P}\|_{\otimes}$$

s.t. $Z^{(v)} \geq 0$, $\text{diag}(Z^{(v)}) = 0$, $Z^{(v)} I = I$, $F^T F = I$,

$0 \leq H_{i,v} \leq 1$, $\sum_{i=1, i \neq v}^V H_{i,v} = 1$, $H_{v,v} = 0$, $Z^{(v)} = P^{(v)}$.

(6)

where $\psi = \{Z^{(v)}, E^{(v)}, F, B^{(v)}, P^{(v)}, H\}$ and $\mathcal{P} \in R^{n \times n \times V}$ denotes a 3-order tensor calculated from $\{P^{(v)}\}_{v=1}^V$.

$Z^{(v)}$ -Step: By fixing the other variables, we can obtain $Z^{(v)}$ by minimizing the following optimization problem:

$$\begin{aligned} \mathcal{L}(Z^{(v)}) = \min_{Z^{(v)}} & \lambda_1 \|Z^{(v)} - \sum_{i=1, i \neq v}^V Z^{(i)} H_{i,v}\|_F^2 \\ & + \frac{\mu}{2} \|Y^{(v)} - Y^{(v)} Z^{(v)} - B^{(v)} + \frac{C_2^{(v)}}{\mu}\|_F^2 \\ & + \frac{\mu}{2} \|Z^{(v)} - P^{(v)} + \frac{C_3^{(v)}}{\mu}\|_F^2 + \frac{\lambda_3}{2} \sum_{i,j}^n Q_{i,j} Z_{i,j}^{(v)} \end{aligned} \quad (7)$$

where $q_{ij} = \|f_{i,:} - f_{j,:}\|_2^2$ denotes the element of Q .

Then, we can attain $\tilde{Z}^{(v)}$ via setting $\partial \mathcal{L} / \partial Z^{(v)} = 0$ as follows:

$$\begin{aligned} \tilde{Z}^{(v)} = & \left(\frac{2\lambda_1(V-1)^2}{V^2} I + \mu I + \mu Y^{(v)T} Y^{(v)} \right)^{-1} \\ & \left(2 \frac{V-1}{V^2} \lambda_1 R^{(v)} + \mu P^{(v)} + \lambda_2 Q - C_3^{(v)} + K^{(v)} \right) \end{aligned} \quad (8)$$

where $R^{(v)} = \sum_{i=1, i \neq v}^V Z^{(i)} H_{i,v}$ and $K^{(v)} = Y^{(v)T} (\mu(Y^{(v)} - B^{(v)}) + C_2^{(v)})$.

Afterwards, we can achieve the optimal $Z^{(i)}$ by solving the following minimization problem:

$$\min_{Z^{(i)} \geq 0, \text{diag}(Z^{(i)})=0, Z^{(i)} I=I} \|Z^{(i)} - \tilde{Z}^{(i)}\|_F^2 \quad (9)$$

Specifically, (9) is independent with respect to all columns. Hence, we can obtain the optimal solution column to column as follows (Zhao et al. 2021; Nie et al. 2016):

$$Z_{i,j}^{(v)} = \begin{cases} (\tilde{Z}_{i,j}^{(v)} + \eta)_+, & i \neq j \\ 0, & i = j \end{cases} \quad (10)$$

where function $(A)_+ = \max(A, 0)$ ensures all elements of A to be non-negative. Otherwise, η can be gained as follows:

$$\eta = \left(1 - \sum_{i=1, i \neq j}^n \tilde{Z}_{i,j}^{(v)} \right) / (n-1) \quad (11)$$

$B^{(v)}$ -Step: By fixing the other variables, we can attain $B^{(v)}$ by solving the following minimization problem:

$$\begin{aligned} \mathcal{L}(B^{(v)}) = \\ \min_{B^{(v)}} \sum_{v=1}^V \|B^{(v)}\|_1 + \frac{\mu}{2} \|Y^{(v)} - Y^{(v)} Z^{(v)} - B^{(v)} + \frac{C_2^{(v)}}{\mu}\|_F^2. \end{aligned} \quad (12)$$

We can solve the sparsity optimization problem (12) as follows:

$$B^{(v)} = \Theta_{\frac{\mu}{2}}(Y^{(v)} - Y^{(v)} Z^{(v)} + \frac{C_2^{(v)}}{\mu}), \quad (13)$$

where Θ denotes the shrinkage operator (Candès et al. 2011; Zhao, Zhang, and Li 2020).

$E^{(v)}$ -Step: By fixing the other variables, we can attain $E^{(v)}$ by solving the following minimization problem:

$$\mathcal{L}(E^{(v)}) = \min_{E^{(v)}} \sum_{v=1}^V \frac{\lambda_2}{2} \|E^{(v)}\|_F^2 + \frac{\mu}{2} \|G_2^{(v)} - E^{(v)} W^{(v)}\|_F^2. \quad (14)$$

where $G_2^{(v)} = Y^{(v)} - X^{(v)} - B^{(v)} + \frac{C_1^{(v)}}{\mu}$.

By setting $\partial \mathcal{L} / \partial E^{(v)} = 0$, we can attain $E^{(v)}$ as follows:

$$E^{(v)} = \mu G_2^{(v)} W^{(v)T} (\lambda_2 + \mu W^{(v)} W^{(v)T})^{-1}. \quad (15)$$

F -Step: By fixing the other variables, F can be obtained by solving the following problem:

$$\mathcal{L}(F) = \lambda_3 \min_F \sum_{v=1}^V \text{Tr}(F^T L_{Z^{(v)}} F) \text{ s.t. } F^T F = I. \quad (16)$$

It can be seen that (16) is an eigenvalue decomposition problem. Then, F can be expressed as $[f_1, f_2, \dots, f_c] \in R^{n \times c}$, where f_1, f_2, \dots, f_c correspond to the first c minimum eigenvalues of $\sum_{v=1}^V L_{Z^{(v)}}$.

H -Step: By fixing the other variables, H can be obtained by solving the following problem:

$$\begin{aligned} \mathcal{L}(H) = \min_H \sum_{v=1}^V \lambda_1 \|Z^{(v)} - \sum_{i=1, i \neq v}^V Z^{(i)} H_{i,v}\|_F^2 \\ \text{s.t. } 0 \leq H_{i,v} \leq 1, \sum_{i=1, i \neq v}^V H_{i,v} = 1, H_{v,v} = 0 \end{aligned} \quad (17)$$

Problem (17) can be simplified as follows:

$$\min_{0 \leq H_{i,v} \leq 1, \sum_{i=1, i \neq v}^V H_{i,v} = 1, H_{v,v} = 0} \sum_{v=1}^V \|U_{:,v} - U H_{:,v}\|_2^2, \quad (18)$$

where $U \in R^{n^2 \times V}$ is a matrix produced from $\{Z^{(v)}\}_{v=1}^V$, whose v th column is the vector stacked by all columns of matrix $Z^{(v)}$.

Problem (18) is a typical simplex representation based optimization problem and can be quickly solved via the accelerated projected gradient method.

$P^{(v)}$ -Step: By fixing the other variables, $P^{(v)}$ can be obtained by solving the following problem:

$$\begin{aligned} \mathcal{L}(P^{(v)}) &= \min_{P^{(v)}} \sum_{v=1}^V \frac{\mu}{2} \|Z^{(v)} - P^{(v)} + \frac{C_3^{(v)}}{\mu}\|_F^2 + \|\mathcal{P}\|_{\otimes} \\ \rightarrow \mathcal{P} &= \min_{\mathcal{P}} \|\mathcal{P}\|_{\otimes} + \frac{\mu}{2} \|\mathcal{Z} - \mathcal{P} + \frac{C}{\mu}\|_F^2 \end{aligned} \quad (19)$$

where $C \in R^{n \times n \times V}$ is a tensor collected by all $\{C_3^{(v)}\}_{v=1}^V$. Problem (19) is a typical t-SVD based tensor nuclear norm minimization problem and has the following closed-form solution:

$$\mathcal{P} = \mathcal{U} \mathcal{K}_{\hat{\mu}}(\mathcal{S}) \mathcal{V}^T \quad (20)$$

where $\hat{\mu} = n\mu$, $\mathcal{Z} + \mathcal{A}/\mu = \mathcal{U} \mathcal{S} \mathcal{V}^T$ is obtained by the t-SVD operation. $\mathcal{K}_{\hat{\mu}} = \mathcal{S} \mathcal{J}$, where $\mathcal{J} \in R^{n \times l \times n}$ is a diagonal tensor whose diagonal elements in the Fourier domain are expressed as $\mathcal{J}_f(i, i, j) = \max(1 - \hat{\mu}/\mathcal{S}_f^{(j)}(i, i), 0)$.

Updated $C_1^{(v)}$, $C_2^{(v)}$, $C_3^{(v)}$, and μ : We gain the Lagrangian multipliers $C_1^{(v)}$, $C_2^{(v)}$, $C_3^{(v)}$, and the parameter μ as follows:

$$C_1^{(v)} = C_1^{(v)} + \mu(Y^{(v)} - X^{(v)} - E^{(v)}W^{(v)}), \quad (21)$$

$$C_2^{(v)} = C_2^{(v)} + \mu(Y^{(v)} - Y^{(v)}Z^{(v)} - B^{(v)}) \quad (22)$$

$$C_3^{(v)} = C_3^{(v)} + \mu(Z^{(v)} - P^{(v)}), \quad (23)$$

$$\mu = \min(\rho\mu, \mu_{max}) \quad (24)$$

where ρ and μ_{max} are two constants.

The detailed optimization processes for each variable in problem (6) are summarized in Algorithm 1.

Computational Complexity Analysis

Since the $Z^{(v)}$ -Step and H -Step only include some simple element-wise operations, the computational cost of these two steps can be neglected. Besides this, due to the fact that the shrinkage operator takes very little computational cost, it also can be neglected in the $B^{(v)}$ -Step. For the $E^{(v)}$ -Step, the time cost for the inverse operation is calculated as $\mathcal{O}(m^3)$. To solve the eigenvalue decomposition problem in the F -Step, a function 'eigs' in (Wright and Trefethen 2001) is applied to accelerate the computing efficiency, which only requires $\mathcal{O}(cn^3)$. In the $P^{(v)}$ -Step, the most time cost incorporates t-SVD as well as FFT and inverse FFT operations, which can be respectively computed as $\mathcal{O}(V^2n^2)$ and $\mathcal{O}(Vn^2 \log(n))$. In accordance with the above analysis, the total time consumption for Algorithm 1 is about $\mathcal{O}(\tau(m^3 + cn^3 + V^2n^2 + Vn^2 \log(n)))$, where τ represents the iteration number.

Algorithm 1: The proposed TIMVC-IGC

- 1: **Input:** Incomplete multi-view data matrix $\{X^{(v)} \in R^{d^{(v)} \times n^{(v)}}\}_{v=1}^V$, parameters of λ_1 , λ_2 , and λ_3 .
 - 2: **Initialization:** Initialize $Z^{(v)}$ via the k-nearest neighbor graph of each view; Initialize F with the eigenvalue decomposition on the Laplacian graph of each transformed complete view; $C_1^{(v)} = 0$, $C_2^{(v)} = 0$; $C_3^{(v)} = 0$; $\mu = 0.1$, $\rho = 1.01$, and $\mu_{max} = 10^8$.
 - 3: **while** iteration $< R$ **do**
 - 4: Update $Z^{(v)}$ using (11).
 - 5: Update $B^{(v)}$ using (13).
 - 6: Update $E^{(v)}$ using (15).
 - 7: Update F using (16).
 - 8: Update H using (18).
 - 9: Update $P^{(v)}$ using (20).
 - 10: Update $C_1^{(v)}$, $C_2^{(v)}$, $C_3^{(v)}$, and μ using (21), (22), (23), and (24), correspondingly.
 - 11: **end**
 - 12: **Output:** $Z^{(v)}$, $B^{(v)}$, $E^{(v)}$, F , H , and $P^{(v)}$.
-

Experiments and Analysis

Database Description

Handwritten Multi-feature Dataset¹ (Handwritten) includes 10 classes, i.e., digits '0-9', where each class contains 200 handwritten samples. Specifically, six types of features, i.e., pixel averages, Fourier coefficients, profile correlations, Zernike moment, Karhunen-love coefficient, and morphological, were extracted from each sample as six views. **The Columbia Object Image Library²** (COIL-20) totally includes 1,440 images from 20 classes. We extracted three types of features, i.e., deep feature of VGG-F (Zhao, Zhang, and Chen 2019), LBP feature (Oliva and Torralba 2001), and vectored pixel feature from each image to construct the multi-view dataset. **Caltech101** database totally consists of 101 objects, where each class contains 40-800 images (Fei-Fei, Fergus, and Perona 2004). In this paper, a subset of Caltech101 containing 1474 images from 7 classes was selected for the comparison experiments. Particularly, the selected multi-view dataset contains two views of GIST and LBP (Li et al. 2015). Referring to (Zhao, Liu, and Fu 2016), a subset of the **BUAA-visnir face database³** (BUAA) was selected to evaluate the proposed method in this study, which contains two views of 90 visual images and 90 near-infrared images of the first 10 classes.

Incomplete multi-view data construction: In this paper, we constructed the incomplete multi-view data by randomly removing $p\%$ ($p = \{10\%, 30\%, 50\%\}$) instances in each view to simulate Case 3 in Fig. 1. For each dataset, each method was performed 10 times and the average value was reported as the final result. Moreover, the clustering accuracy (ACC), normalized mutual information (NMI), and

¹<https://archive.ics.uci.edu/ml/datasets/MultipleFeatures>.

²<http://www.cs.columbia.edu/CAVE/software/softlib/coil-20.php>

³<https://github.com/hdzhao/IMG/tree/master/data>.

Data	Methods	ACC (%)			NMI (%)			Purity (%)		
		0.1	0.3	0.5	0.1	0.3	0.5	0.1	0.3	0.5
Handwrite	BSV	60.80±9.94	41.18±5.05	26.57±2.31	51.44±8.47	35.06±5.22	19.93±2.62	57.76±8.91	42.11±4.71	27.81±2.26
	Concat	61.40±1.10	45.25±0.94	30.85±0.67	55.52±0.92	39.83±1.04	25.13±0.68	61.72±0.76	45.92±0.93	31.74±0.59
	GPMVC	47.03±2.92	34.39±4.82	25.70±1.43	38.59±4.92	26.06±3.39	15.84±1.39	48.55±5.69	35.40±3.21	27.22±2.28
	MIC	53.34±5.99	41.01±2.19	24.87±1.07	48.37±3.89	33.66±3.11	16.64±1.71	55.10±3.84	41.86±2.39	25.90±1.87
	DAIMC	82.79±2.55	78.39±1.11	55.89±5.37	71.80±2.84	64.05±1.89	41.03±3.08	82.79±2.25	78.39±1.11	56.03±5.27
	OMVC	54.53±3.72	39.46±4.97	31.32±2.06	45.51±1.66	30.45±4.03	22.08±2.35	55.23±3.50	40.97±0.80	33.34±2.40
	MVL_IV	49.35±4.35	29.90±2.75	25.50±3.18	47.99±1.70	30.34±2.29	24.13±1.81	50.55±4.35	31.65±0.50	28.25±5.77
	AWIMVC	55.28±1.83	47.69±0.49	23.05±1.39	55.13±2.18	40.33±1.11	22.36±1.08	57.15±1.36	49.02±1.62	83.22±0.50
	UEAF	59.63±2.66	47.55±3.58	24.90±6.22	60.33±5.20	41.94±3.90	22.12±4.58	68.77±3.10	48.95±3.14	25.95±3.99
	AGC_IMVC	85.73±3.75	83.88±2.28	82.25±1.26	85.64±7.89	82.91±1.43	73.14±2.25	86.75±2.76	84.82±2.10	82.64±1.56
	ICSL_IMC	88.10±0.17	83.98±0.65	85.35±3.15	88.14±0.48	86.28±2.45	74.88±0.70	88.10±2.89	86.85±2.89	83.45±1.12
	IMVTSC	99.10±0.09	99.10±0.25	98.89±0.33	99.16±0.28	98.58±0.32	98.01±0.18	99.30±0.07	99.16±0.55	98.96±0.04
TIMVC_IGC	99.90±1.33	99.85±1.13	99.80±0.76	99.73±2.11	99.59±1.82	99.45±2.05	99.90±0.88	99.85±2.73	98.82±1.59	
COIL-20	BSV	41.46±6.90	40.42±3.48	35.97±4.55	53.38±5.57	51.22±4.40	43.08±6.90	46.07±4.66	43.68±2.58	38.42±6.90
	Concat	31.35±2.43	28.89±8.62	22.64±3.83	45.58±1.47	42.34±7.49	35.20±2.28	33.62±2.17	31.11±3.67	24.38±1.99
	GPMVC	38.43±2.89	40.00±8.80	34.72±7.00	49.17±3.37	50.35±3.88	42.72±4.35	40.50±9.90	41.88±4.90	38.12±6.65
	MIC	40.15±4.84	42.63±1.99	32.17±5.86	48.95±8.82	51.33±8.23	46.10±4.61	43.28±7.32	40.10±1.79	39.17±2.07
	DAIMC	84.15±3.11	83.68±1.99	76.25±2.07	90.06±8.86	89.94±2.06	83.71±2.77	86.33±5.71	86.87±8.62	79.24±9.85
	OMVC	49.38±4.35	46.53±3.46	50.19±5.62	61.07±3.13	62.64±1.98	59.51±2.55	54.11±4.32	49.03±2.89	55.40±3.76
	MVL_IV	50.13±0.92	48.54±1.64	52.43±1.15	63.59±1.54	62.81±0.99	63.28±0.85	53.37±3.83	52.78±1.60	56.53±1.21
	AWIMVC	51.02±0.99	46.55±0.71	33.49±1.77	56.90±0.43	50.71±1.90	4.30±1.32	55.21±1.68	41.70±1.61	33.59±1.52
	UEAF	53.66±4.61	47.22±6.20	36.04±3.68	59.88±6.09	52.31±5.96	44.46±6.14	54.37±3.88	48.82±4.91	38.89±8.43
	AGC_IMVC	84.12±1.04	83.54±2.41	76.18±3.96	92.20±1.18	90.13±3.86	83.59±5.55	87.35±2.04	86.94±1.41	79.17±3.77
	ICSL_IMC	85.66±1.27	83.98±0.63	77.25±1.87	93.00±1.26	90.94±1.28	84.93±1.05	87.96±0.85	87.48±0.95	79.94±1.29
	IMVTSC	83.55±0.67	82.18±0.35	81.46±0.15	92.00±0.08	91.09±0.28	90.02±0.20	88.29±0.81	86.35±1.06	85.47±0.12
TIMVC_IGC	87.39±1.12	85.44±0.63	84.00±2.21	94.16±2.08	93.66±2.60	93.24±0.85	89.38±1.80	88.89±1.29	88.71±0.87	

Table 1: ACC (%), NMI (%), and Purity (%) of Different Methods on the Handwritten, and COIL-20 Incomplete Multi-view Datasets.

purity were exploited as the evaluation metrics (Wen et al. 2020a).

Experimental Results and Analysis

In the comparative experiments, the proposed TIMVC_IGC was conducted in comparison with a variety of state-of-the-art and classical IMVC methods, including BSV (Zhao, Liu, and Fu 2016), Concat (Zhao, Liu, and Fu 2016), GPMVC (Rai et al. 2016), MIC (Shao, He, and Yu 2015b), DAIMC (Hu and Chen 2019), OMVC (Shao et al. 2016), MVL_IV (Xu, Tao, and Xu 2015), AWIMVC (Deng et al. 2020), UEAF (Wen et al. 2019), AGC_IMVC (Wen et al. 2020a), ICSL_IMC (Zhao et al. 2021), and tensor-based IMVTSC (Wen et al. 2021). Table 1 and Table 2 report the experimental results on the Handwritten, COIL-20, Caltech101, and BUAA databases. It can be obviously observed that:

(1) The proposed TIMVC_IGC obtains the best clustering performances on different incomplete multi-view databases. For example, our method attains significant improvement of 17.40%, 12.44%, and 13.98% w.r.t. ACC, NMI, and Purity on the BUAA dataset with a missing view rate of 30% in comparison with the tensor-based IMVTSC, which obtains the second best performances.

(2) The TIMVC_IGC, ICSL_IMC, and AGC_IMVC can outperform the other IMVC-based methods in most cases. Since these three methods try to gain the complete graphs of different views by performing missing view completion, the missing information hidden in the missing instances can

be exploited. Specifically, due to the fact that the proposed TIMVC_IGC can explore higher-order correlations between different views, it achieves a better performance than the other methods.

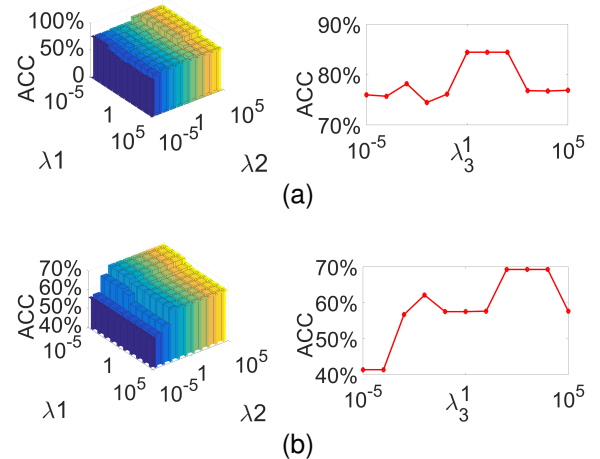


Figure 2: Clustering accuracies versus different combinations of parameters on the (a) COIL-20 and (b) Caltech101 databases, respectively.

Data	Methods	ACC (%)			NMI (%)			Purity (%)		
		0.1	0.3	0.5	0.1	0.3	0.5	0.1	0.3	0.5
Caltech101	BSV	43.89±1.37	39.06±1.26	38.31±1.68	39.66±2.23	31.63±1.51	26.81±1.38	84.08±1.23	75.25±0.71	68.97±0.49
	Concat	41.25±1.67	40.55±1.89	38.06±0.88	43.48±0.92	37.99±2.17	30.28±0.66	84.91±0.50	82.54±1.12	77.56±0.98
	GPMVC	38.43±2.89	40.00±8.80	34.72±7.00	49.17±3.37	50.35±3.88	42.72±4.35	40.50±9.90	41.88±4.90	38.12±6.65
	MIC	44.07±4.97	38.01±2.12	35.80±2.34	33.71±2.66	27.35±1.69	20.44±0.98	78.12±1.76	73.31±0.72	68.26±1.40
	DAIMC	48.29±6.76	47.46±3.42	44.89±4.88	44.61±3.88	38.45±2.88	36.28±2.34	83.32±1.31	76.83±3.23	75.50±1.17
	OMVC	49.38±4.35	46.53±3.46	50.19±5.62	61.07±3.13	62.64±1.98	59.51±2.55	54.11±4.32	49.03±2.89	55.40±3.76
	MVL_IV	50.13±0.92	48.54±1.64	52.43±1.15	63.59±1.54	62.81±0.99	63.28±0.85	53.37±3.83	52.78±1.60	56.53±1.21
	AWIMVC	51.02±0.99	46.55±0.71	33.49±1.77	56.90±0.43	50.71±1.90	44.30±1.32	55.21±1.68	41.70±1.61	33.59±1.52
	UEAF	50.82±4.05	42.71±0.84	36.32±4.22	39.44±2.07	31.07±1.99	24.02±1.37	81.49±1.78	78.26±2.12	76.29±1.93
	AGC.IMVC	59.63±4.11	57.31±2.13	55.10±2.66	59.68±2.55	59.47±1.28	59.37±2.36	84.14±2.24	61.59±2.01	60.22±2.57
	ICSL.IMC	61.33±1.17	60.56±0.83	59.49±1.37	60.98±0.66	59.66±1.28	57.93±1.25	82.12±2.15	62.22±0.75	58.17±1.79
	IMVTSC	64.18±0.49	63.19±2.41	54.17±2.04	55.97±0.71	53.84±2.72	51.37±1.40	89.09±0.52	88.69±1.06	88.19±1.82
TIMVC_IGC	69.27±1.22	67.78±0.69	67.10±1.48	65.26±2.53	64.80±2.11	63.96±1.04	94.03±0.72	93.76±1.74	91.11±1.73	
BUAA	BSV	33.64±6.15	30.02±10.03	26.59±2.71	56.22±3.45	54.29±8.62	46.47±6.14	32.17±5.50	31.62±6.69	28.22±9.78
	Concat	28.43±9.77	26.07±4.02	23.56±8.61	63.61±6.13	60.59±2.07	55.95±7.15	29.88±5.41	27.71±7.40	24.74±8.58
	GPMVC	34.57±8.52	32.29±5.03	27.19±4.74	57.18±9.95	55.34±7.21	47.24±4.97	35.40±5.74	33.63±2.70	28.52±3.48
	MIC	35.63±5.31	34.77±4.97	29.16±3.13	59.65±2.07	55.42±6.07	46.20±3.66	37.10±4.56	36.33±3.10	29.16±3.94
	DAIMC	29.11±1.08	27.41±3.10	25.63±5.31	56.85±3.68	54.39±2.17	57.64±8.62	30.01±5.81	28.74±6.20	26.81±6.69
	OMVC	43.57±7.48	30.61±6.03	28.77±2.23	63.59±2.07	62.17±3.89	54.91±4.39	46.48±5.33	40.10±5.05	37.11±7.18
	MLV_IV	44.07±3.72	36.81±1.16	31.11±0.27	72.00±1.35	66.83±2.53	62.63±0.14	45.48±0.95	38.16±1.01	32.74±0.41
	AWIMVC	47.11±1.50	41.02±1.67	33.27±0.68	72.55±1.66	62.09±1.05	61.22±0.93	48.47±0.89	43.68±0.48	36.49±0.74
	UEAF	35.93±4.30	30.59±3.97	26.74±9.66	66.64±5.27	60.46±7.94	59.14±3.38	37.56±5.20	32.22±4.41	28.07±3.97
	AGC.IMVC	37.26±4.68	26.74±0.67	25.48±2.70	61.51±5.05	53.87±0.61	57.51±5.25	38.96±1.66	28.01±1.37	26.67±3.72
	ICSL.IMC	49.19±1.48	43.41±1.34	36.22±0.58	74.89±0.74	70.21±0.59	63.82±0.14	50.67±1.32	44.59±2.67	38.08±0.35
	IMVTSC	75.21±1.27	55.46±1.25	38.33±2.47	78.54±2.20	73.90±1.62	60.55±2.25	68.20±1.38	58.36±1.81	36.52±2.55
TIMVC_IGC	79.41±1.40	65.11±2.08	41.37±0.95	91.08±0.81	83.09±1.22	65.02±1.40	81.78±2.11	66.52±1.79	42.56±1.61	

Table 2: ACC (%), NMI (%), and Purity (%) of Different Methods on the Caltech101, and BUAA Incomplete Multi-view Datasets.

Parameter Sensitivity Analysis

Three parameters, i.e., λ_1 , λ_2 , and λ_3 need to be adjusted in Algorithm 1. Aiming to select the suitable combination of parameters for each database, a set of experiments were implemented. Fig. 2 depicts the parameter sensitivities of the proposed method on different datasets. It is obvious that our method is insensitive to λ_1 in the range of $[10^{-5}, 10^2]$. In addition, it can be seen that the highest clustering accuracy can be guaranteed for all databases with $\lambda_2 \in [10^2, 10^5]$ and $\lambda_3 = 10^3$.

Convergence Analysis

To prove the convergence property of the proposed method, a group of experiments were implemented to analyze the convergence of TIMVC_IGC. Fig. 3 shows the clustering accuracies and the objective function values (OFV) v.s. the number of iterations on different databases with a missing view rate of 30%. From Fig. 3, it can be obviously observed that the clustering accuracies increase to a stable value after several iterations, where the objective function values monotonically decrease to a denomination after a few of steps. Thus, the convergence property of our method can be proven.

Conclusions

In this paper, a novel and efficient IMVC framework, called TIMVC_IGC, for incomplete multi-view clustering is proposed. To adaptively complete the structure for each view,

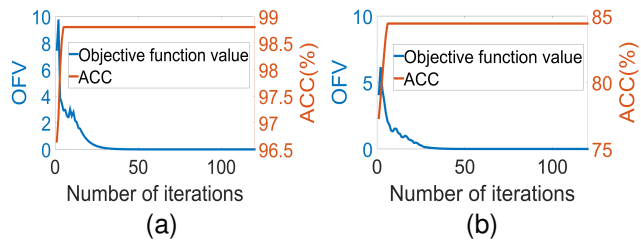


Figure 3: Objective function value and clustering accuracy of the proposed method versus the number of iterations on the (a) Handwritten, and (b) COIL-20 databases, respectively.

TIMVC_IGC jointly considers the missing view inferring and the consistency semantic representation for all views. To this end, a missing view inferring term and a between-view consistency constraint are introduced to infer the missing instances and construct the complete graph for each view. Besides this, TIMVC_IGC simultaneously learns the low-rank structures of different views and explores the high-order correlations between different graphs in a latent manifold subspace using a low-rank tensor constraint. Therefore, the intrinsic structures can be obtained to guarantee the semantic consistency of different views. Experimental results illustrates that TIMVC_IGC can well recover the missing instances and significantly improve the performance.

Acknowledgments

This work was partially supported by the University of Macau (Grant no. MYRG2019-00006-FST), the National Natural Science Foundation of China (Grant nos. 62106052, 62176066, and 62006059), the China Postdoctoral Science Foundation (Grant 2022M710827), and the Science and Technology Development Fund (FDCT) of Macau (Grant no. 0038/2021/APD).

References

- Abhadiomhen, S. E.; Wang, Z.; Shen, X.; and Fan, J. 2021. Multiview common subspace clustering via coupled low rank representation. *ACM Transactions on Intelligent Systems and Technology (TIST)*, 12(4): 1–25.
- Candès, E. J.; Li, X.; Ma, Y.; and Wright, J. 2011. Robust principal component analysis? *Journal of the ACM (JACM)*, 58(3): 1–37.
- Chao, G.; Sun, S.; and Bi, J. 2021. A survey on multiview clustering. *IEEE transactions on artificial intelligence*, 2(2): 146–168.
- Chen, Y.; Xiao, X.; Peng, C.; Lu, G.; and Zhou, Y. 2021. Low-rank tensor graph learning for multi-view subspace clustering. *IEEE Transactions on Circuits and Systems for Video Technology*, 32(1): 92–104.
- Cheng, M.; Jing, L.; and Ng, M. K. 2018. Tensor-based low-dimensional representation learning for multi-view clustering. *IEEE Transactions on Image Processing*, 28(5): 2399–2414.
- Cui, H.; Zhu, L.; Li, J.; Yang, Y.; and Nie, L. 2020. Scalable Deep Hashing for Large-Scale Social Image Retrieval. *IEEE Transactions on Image Processing*, 29: 1271–1284.
- Deng, W.; Liu, L.; Li, J.; and Lin, Y. 2020. Auto-weighted incomplete multi-view clustering. *IEEE Access*, 8: 138752–138762.
- Fei-Fei, L.; Fergus, R.; and Perona, P. 2004. Learning generative visual models from few training examples: An incremental bayesian approach tested on 101 object categories. In *2004 conference on computer vision and pattern recognition workshop*, 178–178. IEEE.
- Gao, H.; Nie, F.; Li, X.; and Huang, H. 2015. Multi-view subspace clustering. In *Proceedings of the IEEE international conference on computer vision*, 4238–4246.
- Gao, H.; Peng, Y.; and Jian, S. 2016. Incomplete multi-view clustering. In *International Conference on Intelligent Information Processing*, 245–255. Springer.
- Hu, M.; and Chen, S. 2019. Doubly aligned incomplete multi-view clustering. *arXiv preprint arXiv:1903.02785*.
- Hu, S.; Lou, Z.; and Ye, Y. 2021. View-Wise Versus Cluster-Wise Weight: Which Is Better for Multi-View Clustering? *IEEE Transactions on Image Processing*, 31: 58–71.
- Hu, S.; Shi, Z.; and Ye, Y. 2020. DMIB: Dual-correlated multivariate information bottleneck for multiview clustering. *IEEE Transactions on Cybernetics*.
- Huang, S.; Zhang, H.; and Pižurica, A. 2021. Hybrid-hypergraph regularized multiview subspace clustering for hyperspectral images. *IEEE Transactions on Geoscience and Remote Sensing*, 60: 1–16.
- Jia, Y.; Liu, H.; Hou, J.; Kwong, S.; and Zhang, Q. 2021. Multi-view spectral clustering tailored tensor low-rank representation. *IEEE Transactions on Circuits and Systems for Video Technology*, 31(12): 4784–4797.
- Li, L.; and He, H. 2020. Bipartite graph based multi-view clustering. *IEEE Transactions on Knowledge and Data Engineering*.
- Li, L.; Wan, Z.; and He, H. 2021. Incomplete multi-view clustering with joint partition and graph learning. *IEEE Transactions on Knowledge and Data Engineering*.
- Li, S.-Y.; Jiang, Y.; and Zhou, Z.-H. 2014. Partial multi-view clustering. In *Proceedings of the AAAI conference on artificial intelligence*, volume 28.
- Li, Y.; Nie, F.; Huang, H.; and Huang, J. 2015. Large-scale multi-view spectral clustering via bipartite graph. In *Twenty-ninth AAAI conference on artificial intelligence*.
- Liu, Z.; Li, Y.; Yao, L.; Wang, X.; and Nie, F. 2021. Agglomerative neural networks for multiview clustering. *IEEE Transactions on Neural Networks and Learning Systems*.
- Lu, X.; Zhu, L.; Cheng, Z.; Nie, L.; and Zhang, H. 2019. On-line Multi-modal Hashing with Dynamic Query-adaption. In *Proceedings of the 42nd International ACM SIGIR Conference on Research and Development in Information Retrieval (SIGIR)*, 715–724.
- Mitra, V.; Wang, W.; Bartels, C.; Franco, H.; and Vergyri, D. 2018. Articulatory information and multiview features for large vocabulary continuous speech recognition. In *2018 IEEE International Conference on Acoustics, Speech and Signal Processing (ICASSP)*, 5634–5638. IEEE.
- Nie, F.; Wang, X.; Jordan, M.; and Huang, H. 2016. The constrained laplacian rank algorithm for graph-based clustering. In *Proceedings of the AAAI conference on artificial intelligence*, volume 30.
- Oliva, A.; and Torralba, A. 2001. Modeling the shape of the scene: A holistic representation of the spatial envelope. *International journal of computer vision*, 42(3): 145–175.
- Pan, E.; and Kang, Z. 2021. Multi-view contrastive graph clustering. *Advances in neural information processing systems*, 34: 2148–2159.
- Rai, N.; Negi, S.; Chaudhury, S.; and Deshmukh, O. 2016. Partial multi-view clustering using graph regularized NMF. In *2016 23rd International Conference on Pattern Recognition (ICPR)*, 2192–2197. IEEE.
- Shao, W.; He, L.; Lu, C.-t.; and Philip, S. Y. 2016. Online multi-view clustering with incomplete views. In *2016 IEEE International conference on big data (Big Data)*, 1012–1017. IEEE.
- Shao, W.; He, L.; and Yu, P. S. 2015a. Multiple incomplete views clustering via weighted nonnegative matrix factorization with $l_{2,1}$ regularization. In *Joint European conference on machine learning and knowledge discovery in databases*, 318–334. Springer.

- Shao, W.; He, L.; and Yu, P. S. 2015b. Multiple incomplete views clustering via weighted nonnegative matrix factorization with $l_{2,1}$ regularization. In *Joint European conference on machine learning and knowledge discovery in databases*, 318–334. Springer.
- Sharma, K. K.; and Seal, A. 2021. Multi-view spectral clustering for uncertain objects. *Information Sciences*, 547: 723–745.
- Tao, H.; Hou, C.; Yi, D.; and Zhu, J. 2018. Multiview classification with cohesion and diversity. *IEEE transactions on cybernetics*, 50(5): 2124–2137.
- Wang, H.; Zong, L.; Liu, B.; Yang, Y.; and Zhou, W. 2019. Spectral perturbation meets incomplete multi-view data. *arXiv preprint arXiv:1906.00098*.
- Wang, Q.; Ding, Z.; Tao, Z.; Gao, Q.; and Fu, Y. 2021a. Generative partial multi-view clustering with adaptive fusion and cycle consistency. *IEEE Transactions on Image Processing*, 30: 1771–1783.
- Wang, S.; Liu, X.; Zhu, X.; Zhang, P.; Zhang, Y.; Gao, F.; and Zhu, E. 2021b. Fast parameter-free multi-view subspace clustering with consensus anchor guidance. *IEEE Transactions on Image Processing*, 31: 556–568.
- Wang, Y.; Wu, L.; Lin, X.; and Gao, J. 2018. Multiview spectral clustering via structured low-rank matrix factorization. *IEEE transactions on neural networks and learning systems*, 29(10): 4833–4843.
- Wen, J.; Xu, Y.; and Liu, H. 2018. Incomplete multiview spectral clustering with adaptive graph learning. *IEEE transactions on cybernetics*, 50(4): 1418–1429.
- Wen, J.; Yan, K.; Zhang, Z.; Xu, Y.; Wang, J.; Fei, L.; and Zhang, B. 2020a. Adaptive graph completion based incomplete multi-view clustering. *IEEE Transactions on Multimedia*, 23: 2493–2504.
- Wen, J.; Zhang, Z.; Fei, L.; Zhang, B.; Xu, Y.; Zhang, Z.; and Li, J. 2022. A survey on incomplete multiview clustering. *IEEE Transactions on Systems, Man, and Cybernetics: Systems*.
- Wen, J.; Zhang, Z.; Xu, Y.; Zhang, B.; Fei, L.; and Liu, H. 2019. Unified embedding alignment with missing views inferring for incomplete multi-view clustering. In *Proceedings of the AAAI conference on artificial intelligence*, volume 33, 5393–5400.
- Wen, J.; Zhang, Z.; Zhang, Z.; Fei, L.; and Wang, M. 2020b. Generalized incomplete multiview clustering with flexible locality structure diffusion. *IEEE transactions on cybernetics*, 51(1): 101–114.
- Wen, J.; Zhang, Z.; Zhang, Z.; Zhu, L.; Fei, L.; Zhang, B.; and Xu, Y. 2021. Unified tensor framework for incomplete multi-view clustering and missing-view inferring. In *Proceedings of the AAAI conference on artificial intelligence*, volume 35, 10273–10281.
- Wright, T. G.; and Trefethen, L. N. 2001. Large-scale computation of pseudospectra using ARPACK and eigs. *SIAM Journal on Scientific Computing*, 23(2): 591–605.
- Wu, D.; Nie, F.; Dong, X.; Wang, R.; and Li, X. 2021. Parameter-free consensus embedding learning for multiview graph-based clustering. *IEEE Transactions on Neural Networks and Learning Systems*.
- Wu, J.; Xie, X.; Nie, L.; Lin, Z.; and Zha, H. 2020. Unified graph and low-rank tensor learning for multi-view clustering. In *Proceedings of the AAAI conference on artificial intelligence*, volume 34, 6388–6395.
- Xia, W.; Gao, Q.; Wang, Q.; and Gao, X. 2022. Tensor completion-based incomplete multiview clustering. *IEEE Transactions on Cybernetics*.
- Xu, C.; Liu, H.; Guan, Z.; Wu, X.; Tan, J.; and Ling, B. 2021. Adversarial incomplete multiview subspace clustering networks. *IEEE Transactions on Cybernetics*.
- Xu, C.; Tao, D.; and Xu, C. 2015. Multi-view learning with incomplete views. *IEEE Transactions on Image Processing*, 24(12): 5812–5825.
- Xu, C.; Zhao, W.; Zhao, J.; Guan, Z.; Song, X.; and Li, J. 2022. Uncertainty-aware multi-view deep learning for internet of things applications. *IEEE Transactions on Industrial Informatics*.
- Zhang, C.; Fu, H.; Wang, J.; Li, W.; Cao, X.; and Hu, Q. 2020. Tensorized multi-view subspace representation learning. *International Journal of Computer Vision*, 128(8): 2344–2361.
- Zhang, X.; Liu, H.; Zhang, X.; and Liu, X. 2022. Attributed graph clustering with multi-task embedding learning. *Neural Networks*, 152: 224–233.
- Zhang, Y.; Huang, Q.; Zhang, B.; He, S.; Dan, T.; Peng, H.; and Cai, H. 2021. Deep multiview clustering via iteratively self-supervised universal and specific space learning. *IEEE Transactions on Cybernetics*.
- Zhang, Z.; Lai, Z.; Xu, Y.; Shao, L.; Wu, J.; and Xie, G.-S. 2017. Discriminative elastic-net regularized linear regression. *IEEE Transactions on Image Processing*, 26(3): 1466–1481.
- Zhao, H.; Liu, H.; and Fu, Y. 2016. Incomplete multi-modal visual data grouping. In *IJCAI*, 2392–2398.
- Zhao, S.; Fei, L.; Wen, J.; Wu, J.; and Zhang, B. 2021. Intrinsic and Complete Structure Learning Based Incomplete Multiview Clustering. *IEEE Transactions on Multimedia*.
- Zhao, S.; Zhang, B.; and Chen, C. P. 2019. Joint deep convolutional feature representation for hyperspectral palmprint recognition. *Information Sciences*, 489: 167–181.
- Zhao, S.; Zhang, B.; and Li, S. 2020. Discriminant and sparsity based least squares regression with l_1 regularization for feature representation. In *ICASSP 2020-2020 IEEE International Conference on Acoustics, Speech and Signal Processing (ICASSP)*, 1504–1508. IEEE.
- Zhu, X.; Zhang, S.; He, W.; Hu, R.; Lei, C.; and Zhu, P. 2018. One-step multi-view spectral clustering. *IEEE Transactions on Knowledge and Data Engineering*, 31(10): 2022–2034.
- Zhu, Y.; Ma, J.; Yuan, C.; and Zhu, X. 2022. Interpretable learning based Dynamic Graph Convolutional Networks for Alzheimer’s Disease analysis. *Information Fusion*, 77: 53–61.